Chemical Geology 270 (2010) 110–116

Contents lists available at ScienceDirect

Chemical Geology

journal homepage: www.elsevier.com/locate/chemgeo

Characterizing magnetism of individual magnetosomes by X-ray magnetic circular dichroism in a scanning transmission X-ray microscope

Karen P. Lam [a], Adam P. Hitchcock [a,*], Martin Obst [a,1], John R. Lawrence [b], George D.W. Swerhone [b], Gary G. Leppard [c], Tolek Tyliszczak [d], Chithra Karunakaran [e], Jian Wang [e], Konstantin Kaznatcheev [e], Dennis A. Bazylinski [f], Ulysses Lins [g]

[a] Brockhouse Institute for Materials Research, McMaster University, Hamilton, ON, Canada L8S 4M1
[b] Environment Canada, National Water Research Institute, Saskatoon, SK, Canada S7N 3H5
[c] Environment Canada, National Water Research Institute, Burlington, ON, Canada L7R 4A6
[d] Advanced Light Source, Lawrence Berkeley National Laboratory, Berkeley, CA, 94720, USA
[e] Canadian Light Source Inc., University of Saskatchewan, Saskatoon, SK, Canada S7N 5C6
[f] School of Life Sciences, University of Nevada at Las Vegas, Las Vegas, NV, 89154-4004, USA
[g] Departamento de Microbiologia Geral, Instituto de Microbiologia Professor Paulo de Góes, Universidade Federal do Rio de Janeiro, 21941-590, Rio de Janeiro, RJ, Brazil

ARTICLE INFO

Article history:
Received 14 August 2009
Received in revised form 16 November 2009
Accepted 16 November 2009

Editor: J. Fein

Keywords:
X-ray magnetic circular dichroism
XMCD
Scanning Transmission X-Ray Microscopy
STXM
Magnetotactic bacteria
Magnetosomes
Magnetite
Fe_3O_4
Marine vibrio
Strain MV-1

ABSTRACT

Soft X-ray scanning transmission X-ray microscopy (STXM) was used to measure the Fe $L_{2,3}$ X-ray magnetic circular dichroism (XMCD) signal from individual, 30 nm diameter magnetosomes in a magnetotactic bacterium, specifically the marine vibrio strain MV-1. The Fe $L_{2,3}$ spectra recorded with circularly polarized X-rays from an elliptically polarizing undulator were very similar in shape and magnitude to those of fully saturated magnetite (Fe_3O_4). As previously determined by other techniques, our results show that the magnetic moments of individual magnetosomes arranged in linear chains in intact cells of strain MV-1 are all oriented in the same direction. The magnitude of the XMCD signal averaged over a chain of 9 magnetosomes in one cell is similar to that of single crystal magnetite. The spectral shape is slightly different, and indicates that magnetosomes have excess $Fe^{(II)}$, as noted in previous bulk studies of biogenic magnetite. To our knowledge, this is the first measurement of the XMCD of individual magnetosomes in magnetotactic bacteria.

1. Introduction

Magnetotactic bacteria (MTB) are Gram-negative, motile, aquatic and microaerophilic/anaerobic bacteria, found in both freshwater and marine environments, that migrate with respect to the earth's magnetic field (approximately 0.5 G) in a phenomenon called magnetotaxis (Blakemore, 1975, 1982). The magnetic behaviour of these organisms is associated with intracellularly synthesized magnetic nano-crystals enclosed within membrane vesicles (Frankel and Blakemore, 1980), referred to as magnetosomes (Balkwill et al., 1980). The magnetosome mineral phase consists of single crystals of either the ferrimagnetic iron oxide, magnetite (Fe_3O_4) (Frankel et al., 1979), or the iron sulfide, greigite (Fe_3S_4) (Heywood et al., 1991). The size of magnetosome crystals, regardless of whether they consist of magnetite or greigite, depends on the species of MTB and generally ranges from 35–120 nm (Bazylinski and Frankel, 2004). This is the size range where magnetite crystals are expected to be limited to a single magnetic domain (Dunlop, 1973; Butler and Banerjee, 1975; Kirschvink and Lowenstam, 1979; Muxworthy and Williams, 2006).

Magnetosomes have uniform, species-specific crystal habits with narrow size distributions (Devouard et al., 1998; Arato et al., 2005; Lins et al., 2005), features consistent with a biologically-controlled mineralization process (biomineralization) (Bazylinski and Frankel, 2003). Recent genetic studies confirm that the formation and arrangement of magnetosomes in magnetotactic bacteria is strongly biologically regulated (Komeili et al., 2004, 2006; Scheffel et al., 2006) although there is also evidence that environmental factors also play a

* Corresponding author. Tel.: +1 905 525 9140.
E-mail address: aph@mcmaster.ca (A.P. Hitchcock).
[1] Now Center for Applied Geoscience, Eberhard Karls University, 72076 Tuebingen, Germany.

0009-2541/$ – see front matter © 2009 Elsevier B.V. All rights reserved.
doi:10.1016/j.chemgeo.2009.11.009

role in the biomineralization of magnetite and greigite by magnetotactic bacteria (Blakemore et al., 1985; Bazylinski, 1996; Schüler and Baeuerlein, 1998; Bazylinski et al., 2004). Various methods of examining the chemistry, crystallography and magnetism of the magnetic materials associated with individual cells of magnetotactic bacteria or individual or chains of magnetosomes have great potential to advance the fields of magnetism, magnetic materials and biomineralization. The narrow size and shape distribution of magnetosomes has led to their consideration as candidate materials in technological, medical and environmental applications, such as magnetic recording media, ferrofluids, and magnetic resonance imaging (MRI) (Lee et al., 2005) as well as removal of Au(III) from wastewater (Song et al., 2008). Mimicking the biogenic mineralization process, uniform, superparamagnetic magnetite nano-crystals were successfully synthesized using specific proteins from magnetotactic bacteria in order to control crystal size and habit (Prozorov et al., 2007). Most recently, magnetotactic bacteria have been studied as controlled, MRI-trackable propulsion and steering systems for medical nanorobots operating in the human microvasculature (Martel et al., 2009).

Nanoscale magnetite crystals also have environmental significance. In some deep sea and freshwater lake sediments and soils, fossil bacterial magnetite appears to be the main carrier of natural remnant magnetization (e.g., Petersen et al., 1986; Kim et al., 2005) suggesting that in natural environments the biogenic formation of magnetosomes contributes significantly to the magnetic susceptibility of soils and sediments (Oldfield, 2007). Moreover, the presence of fossil magnetosomes, so-called magnetofossils, has been used as a biomarker for the past presence of magnetotactic bacteria on ancient Earth (Chang et al., 1989) and Mars (Thomas-Keprta et al., 2002).

Many different magnetic techniques have been applied to study biogenic magnetic minerals, including magnetic force microscopy (MFM) (Albrecht et al., 2005), low-temperature SQUID magnetometry (Moskowitz et al., 1993), ferromagnetic resonance (Weiss et al., 2004), and coercivity deconvolution (Egli, 2004). In addition, off-axis electron holography in the transmission electron microscope (TEM) using a Lorentz lens has been applied to visualize the magnetic microstructure of magnetosome chains (Dunin-Borkowski et al., 1998; McCartney et al., 2001; Simpson et al., 2005). X-ray magnetic circular dichroism (XMCD) (Stöhr, 1999) is a synchrotron-based technique that provides an element and site specific probe of magnetism. XMCD uses circularly polarized X-rays to measure the magnitude of the projection of the magnetic moment on the propagation direction of the X-rays. Sette et al. (1990), provided one of the earliest reports of the XMCD spectrum of magnetite. Many other studies of the XMCD of magnetite have been conducted (Kuiper et al., 1997; de Castro et al., 2001; Pattrick et al., 2002; Chen et al., 2004; Huang et al., 2004; Pearce et al., 2006; Goering et al., 2006, 2007; Yamasaki et al., 2009). Recently XMCD has been applied to greigite (Letard et al., 2005), to comparison studies involving biogenic and abiogenic nano-magnetite (Coker et al., 2007; Carvallo et al., 2008) and to the monitoring of *in-vivo* formation of magnetosomes in *Magnetospirillum gryphiswaldense* strain MSR-1 (Staniland et al., 2007).

The Fe L_3 ($2p_{3/2}$) XMCD spectrum of magnetite (Goering et al., 2006, 2007) shows three characteristic peaks. The detailed structure is related to the presence of Fe ions in three distinct sites (Pattrick et al., 2002). Specifically, the sites corresponding to the three peaks in the XMCD spectrum of magnetite are: d^6 O_h (octahedral Fe^{2+} site, 708.1 eV), d^5 T_d (tetrahedral Fe^{3+} site, 709.1 eV) and d^5 O_h (octahedral Fe^{3+} site, 709.9 eV). The negative–positive–negative sense of these contributions is the result of the antiferromagnetic coupling between the spins on the O_h and T_d sites (Brice-Profeta et al., 2005). The site occupancies (relative amounts of Fe present in the three sites) in a given magnetite sample can be obtained from the relative intensities of these signals. Comparisons of the experimental XMCD spectrum with that calculated using ligand field atomic multiplet theory have shown that the proportion of magnetic contributions from the $Fe^{2+}(O_h)$: $Fe^{3+}(T_d)$: $Fe^{3+}(O_h)$ in fully magnetically saturated magnetite is nearly 1:1:1 (Morrall et al., 2003; Carvallo et al., 2008). Thus accurate measurements of XMCD from biologically generated magnetite can be used to deduce information about biomineralization mechanisms and possible biochemical control of inorganic crystallization.

Scanning transmission X-ray microscopy (STXM) allows measurements of spatially-resolved near-edge X-ray absorption fine structure (NEXAFS) spectra with ~30 nm spatial resolution (Howells et al., 2007; Ade and Hitchcock, 2008). STXMs on beamlines equipped with an elliptically polarizing undulator (EPU) allow measurements of XMCD, and thus provide a means to characterize magnetic materials such as magnetosomes at high spatial resolution. In addition, if XMCD at Fe $L_{2,3}$ edges is combined with studies of the biochemical components at the K-edges of C, N, O and the Ca L-edge, etc. (Hitchcock et al., 2005), it is possible to place the magnetic results in the context of the local biochemistry. We believe a program of research of this type offers good prospects to further understand biomineralization processes in magnetotactic bacteria and other organisms. In this initial study, we demonstrate the potential by measuring the magnetic properties of individual magnetosome chains, and individual magnetosomes in the magnetotactic marine vibrio, strain MV-1. This is the first report of an XMCD measurement of the magnetism of individual magnetosomes in intact cells to our knowledge.

2. Materials and methods

2.1. Growth and preparation of bacteria

Cells of the marine magnetotactic vibrio strain MV-1 were grown as previously described (Dean and Bazylinski, 1999). Three ml of a liquid culture of the organism was centrifuged at 4 °C at 10,000 *g* and washed twice in artificial sea water (Bazylinski et al., 2004). A drop (5–10 μL) of the washed cells was deposited onto 200 mesh glow discharged copper grids coated with a thin layer of carbon (~3 nm, TedPella Inc. Catalog # 01822, www.tedpella.com). The drop was left to stand for 1 min prior to removing excess liquid by placing the grid over a filter paper, followed by air-drying the samples.

2.2. Fe $L_{2,3}$ X-ray magnetic circular dichroism (XMCD)

Fe $L_{2,3}$ X-ray absorption spectra were measured using the STXM at BL 10ID1, the soft X-ray spectromicroscopy (SM) beamline of the Canadian Light Source (CLS, Saskatoon, Canada). The source point for the CLS-STXM is an elliptically polarizing undulator (EPU) which provides nearly 100% circularly polarized light at the Fe $L_{2,3}$ edge (Kaznatcheev et al., 2007). Fe $L_{2,3}$ spectra recorded in different runs at the CLS-STXM were found to have energy shifts of up to 0.5 eV, with respect to each other. The absolute energy scale of the spectra was thus determined by shifting it to give the best match to the shape of the Fe $L_{2,3}$ spectrum of magnetite (with appropriate circular polarization) (Goering et al., 2006, 2007). Data was collected in transmission mode by acquiring sequences of images over a range of X-ray energies (image sequence or "stack" mode – Jacobsen et al., 2000). The transmission signals were converted to optical densities (absorbance) using incident flux signals measured through regions a few microns off the MV-1 bacterium under study. In order to obtain adequate statistical quality, we used extensive over-sampling (6 or 8 nm pixel sizes, even though the X-ray spot size is 30 nm) and long dwell times (5–8 ms/pixels, in contrast to typical acquisitions of 0.5–1.0 ms/pixel).

In order to determine the Fe $L_{2,3}$ XMCD, spectra and images were recorded with right circularly polarized (RCP) and left circularly polarized (LCP) X-rays. An additional magnetic field was not applied, and thus we are measuring remnant magnetization. The magnetic moment of intact magnetosome chains is known to lie in the plane of the cell (Simpson et al., 2005). Since XMCD measures the component

of magnetization parallel to the direction of the X-ray beam, measurements were made with the sample mounted such that the plane of the sample was at 60° relative to the incident beam direction. Some measurements were made with the sample plane at 90° to the X-ray beam (conventional STXM geometry), where the XMCD signal was found to be extremely weak, confirming that the magnetic moment lies in the plane of the cells, which lie flat on the support surface. The XMCD signal is dependent on the directionality of the magnetic moment or the spatial orientation of the magnetic dipole being measured. To confirm the dependence of the XMCD signal on the directionality of magnetic moments, the MV-1 sample (still maintained at a 60-degree tilt relative to the X-ray propagation direction) was rotated by 180°. Measurements were then repeated on the same region at both circular polarizations. After this sample rotation, the distinct spectral signatures were interchanged — the spectrum measured with RCP light prior to rotation was the same as that measured by LCP light after rotation, and vice versa. XMCD thus provides the capability to map both the direction and magnitude of magnetic moments in a sample. In addition, since multiple crystal sites contribute to the magnetism of magnetite and their individual XMCD spectral contributions are well resolved (Pattrick et al., 2002), it is possible to vector map the magnetization of the individual sites.

At the time measurements were made, the conventional back-and-forth alternation between RCP and LCP at each photon energy was not possible at the CLS SM-beamline due to limitations of the EPU control system and interference with other ring insertion devices. It is anticipated that use of this mode will further improve the quality and thus sensitivity of our XMCD results.

2.3. Data analysis

Although the CLS-STXM is equipped with an interferometric control system (Kilcoyne et al., 2003) which stabilizes the region under study as the energy is scanned, there is always a small amount of residual drift in the images from energy to energy, as we are pushing the instrument to its limits in this study. The measured RCP and LCP image sequences were combined into a single file, and then aligned using a combination of Fourier transform cross-correlation and manual alignment. Careful inspection of each image sequence to ensure proper alignment was essential to detect meaningful XMCD signal from the individual magnetosomes. The quality of alignment was monitored by summing images in the region of the $2p \rightarrow 3d$ resonances. Multiple alignments were carried out as needed until the halo-like regions of misalignment surrounding the magnetosomes were minimized. The XMCD from individual magnetosomes was extracted by using thresholding techniques to select signal only from the magnetosome (typically 15–20 pixels). Data analysis was performed using aXis2000.[2]

3. Results

The TEM grid with the deposited MV-1 cells was mounted on a polar rotation stage (Johansson et al., 2007) and the plane of the sample was oriented at 60° relative to the X-ray direction. Images at the carbon K-edge (1s, 288.1 eV) revealed the presence of intact cells (Fig 1a) with the curved-rod morphology typical of strain MV-1. The C and O K-edge spectroscopy of the cells revealed the protein-like spectral signatures characteristic of biological materials. The occasional 'blobs' (red in Fig. 1a), which had only a weak C 1s signal and no O 1s signal, are residual salts from the artificial sea water used to wash the sample. Imaging with higher magnification at 709 eV (Fig. 1b) revealed discrete Fe particles aligned in chains inside many, but not all, of the MV-1 cells. The absence of magnetosome chains in some cells is likely due to mutations which form non-magnetic vibrio sp. strains (Dubbels et al., 2004). A region containing both horizontally and vertically aligned magnetosome chains (Fig. 2a) was selected as the focus of our investigation. Fig. 2b, which shows the magnetosomes more clearly, displays the average of 10 images from 706–708 eV minus the average of the Fe pre-edge images from 697–704 eV, both taken from the LCP image sequence. An expanded view of 2 magnetosomes from the sum of images in the Fe L_3 peak (different sample) is shown in Fig. 2c. Fig. 2d shows a 3-D presentation of the signal in Fig. 2c to illustrate the spatial resolution and ability of the STXM to acquire signal from individual magnetosomes.

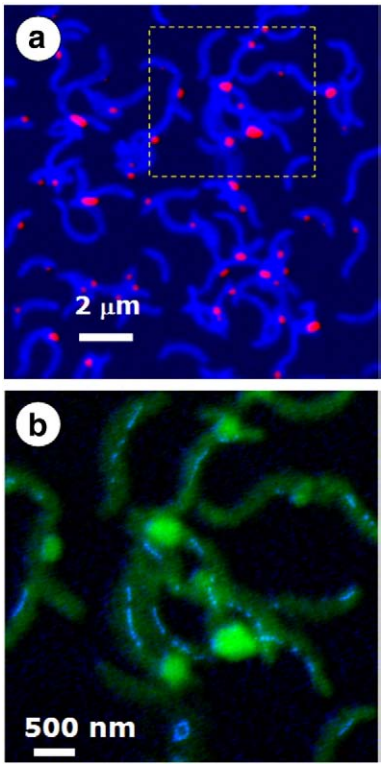

Fig. 1. (Upper) Color composite of two STXM images (optical density, OD) of intact cells of strain MV-1 in the C 1s edge — 280 eV (red) and 288 eV (blue). (Lower) Fe $L_{2,3}$ map ($OD_{709\ eV} - OD_{702\ eV}$, blue = Fe) of the sub-region of the upper image defined by the dotted line, superimposed on the OD image at 702 eV (green = organic matter).

Fig. 3 plots the average Fe $L_{2,3}$ signal from the horizontal chain of magnetosomes in Fig. 2, recorded with the polarization vector of the light parallel to the magnetic vector of the chain (RCP for the sample orientation and magnetic moment of this chain) and with the polarization vector of the light anti-parallel to the magnetic vector of the chain (LCP), in each case compared with the corresponding spectrum of magnetite (Goering et al., 2006, 2007). There is very good agreement in the shapes of the Fe L_3 signal and good, but not exact agreement for the Fe L_2 signal. As shown by Kuiper et al. (1997) and Arenholz et al. (2006), magnetite also exhibits a linear magnetic dichroism (XMLD) signal which could affect these results since the experimental geometry is such that there is a component of z linear polarized light in both the right and left circular polarized measurements. However the magnitude of the XMLD signal is less than 30% of the XMCD signal, and will only be partially exhibited given the experimental geometry. Thus, while there will be a small change from the results of a measurement of the Fe $L_{2,3}$ spectrum without XMLD, this is likely at the level of our statistical uncertainty. Further this will not affect the measured XMCD signal since the linear dichroic effect is constant for both circular polarizations.

[2] aXis2000 is written in Interactive Data Language (IDL). It is available free for noncommercial use from http://unicorn.mcmaster.ca/aXis2000.html.

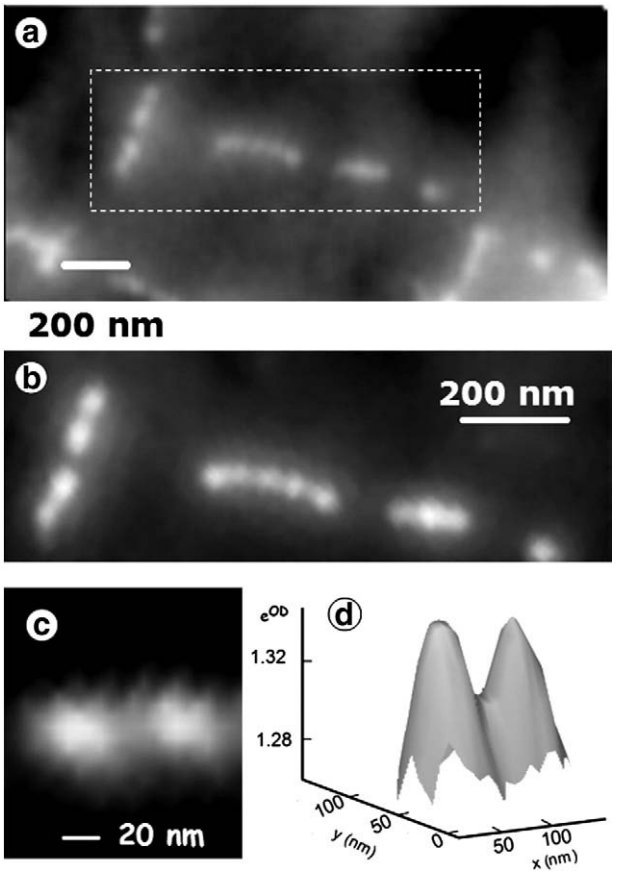

Fig. 2. (a) Fe $L_{2,3}$ optical density image at 709.3 eV of several MV-1 magnetosome chains (recorded with horizontal linear polarization). The sample is in a region free of applied magnetic field, rotated such that the plane of the TEM grid is at 60° to the X-ray beam direction. (b) Sum of 10 OD images in the region of the Fe L_3 peak (706–708 eV) minus the sum of 14 images in the pre-Fe $L_{2,3}$ region (697–704 eV). (c) Expansion of the Fe $L_{2,3}$ image of two MV-1 magnetosomes (different region of the same sample) showing that each is 30 nm in diameter, with a 53 nm centre-to-centre spacing. (d) 3D presentation of the signal in 3c, using an e^{OD} scaling showing distinct resolution of adjacent magnetosomes at the 8% contrast level, consistent with the spatial resolution predicted for zone plates with 25 nm outer zones. All images in this figure have been smoothed using a 3 point Savitsky–Golay procedure.

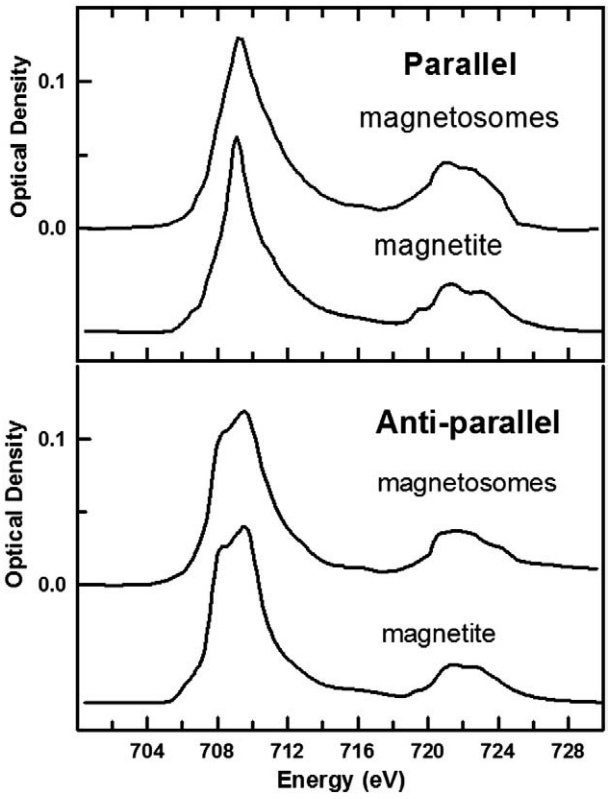

Fig. 3. Fe $L_{2,3}$ spectrum of nine magnetosomes from one horizontal chain (see insert to Fig. 4), recorded with circularly polarized light parallel (red) and anti-parallel (green) to the magnetic moment of the sample, compared to that of magnetite (Goering et al., 2007), rescaled to match the intensities of the magnetosome chain. A linear background, corresponding to the signal from the non-Fe component, has been subtracted.

An overlap plot of the parallel and anti-parallel spectra is shown in Fig. 4. The insert image indicates the 9 magnetosomes from which this signal was obtained. The XMCD signal, the difference (parallel – anti-parallel) of these spectra, is plotted in the lower panel of Fig. 4, in comparison to the published XMCD signal from single crystal magnetite (Goering et al., 2006, 2007). The XMCD intensity scale for both the magnetosome and magnetite data is based on normalizing the Fe $L_{2,3}$ edge jump ($I_{730} - I_{702}$) to unity. At the sample geometry used, 50% of the in-plane magnetic moment is projected onto the X-ray propagation axis. Thus, if these magnetosomes had the same magnetization as bulk magnetite and the moment was fully in the plane of the grid, the XMCD signal from this magnetosome chain would be 50% that of the bulk magnetite. For this reason, the intensity of the XMCD spectrum of abiotic bulk magnetite in the lower panel of Fig. 4 has been reduced by a factor of 2. The Fe L_3 XMCD signal of the magnetosomes is in generally good agreement in both shape and magnitude with that of magnetite. However, the first XMCD structure at 708 eV is more intense relative to that of the 709 and 710 eV features, as compared to that found in the XMCD of bulk magnetite (Goering et al., 2006, 2007). An increase in the signal of the 708 eV peak in the Fe L_3 spectrum of biogenic magnetite has been observed previously both in species that produce it intracellularly, as seen in *M. gryphiswaldense* (Coker et al., 2007), and extracellularly, as seen in *Shewanella putrefaciens* (Carvallo

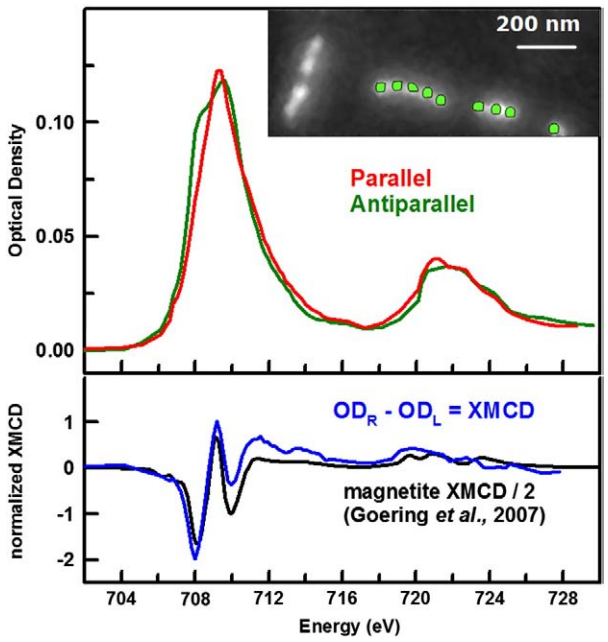

Fig. 4. (Upper) Overplot of the average spectra of 9 magnetosomes in a horizontal chain (see insert image) recorded with circularly polarized X-rays parallel (red) and anti-parallel (green) to the magnetic moment of the sample. The intensity has been scaled such that Fe $L_{2,3}$ edge jump ($I_{730} - I_{702}$) is normalized to 1. (Lower) Comparison of the resulting XMCD of the magnetosome to that of magnetite (Goering et al., 2007). The intensity scale for the XMCD of the magnetosomes is the same as that for the jump-normalized spectra in the upper plot, while that of magnetite was multiplied by 0.50.

et al., 2008) and *Geobacter sulfurreducens* (Coker et al., 2009). Coker et al. (2007, 2009) attributed the increased intensity of the 708 eV peak to non-stoichiometry, in particular excess $Fe^{(II)}$, which could occur if the bio-magnetite is under-oxidized in the anoxic environment. The occupancy ratios of the three components may be determined using fitting methods, by means of non-linear least-squares analysis using calculated spectra for each Fe site, that have been well-established by Pattrick et al. (2002) for a variety of spinel ferrites. The shape and magnitude of the Fe L_2 XMCD signal measured from the magnetosome chain is in less good agreement with that of magnetite, which is most likely a reflection of the limitations of the statistical precision of our present results. Higher precision is needed in the STXM-XMCD measurements to correctly reproduce the much weaker Fe L_2 XMCD structures.

Fe L_3 spectra recorded with right and left circularly polarized light from each of four individual magnetosomes in the horizontal chain are shown in Fig. 5, along with the derived XMCD, in comparison to that of abiotic magnetite. While the precision is not as good as in the spectrum averaged over all 9 magnetosomes in one chain, the Fe L_3 XMCD signal is detected, and it clearly shows the characteristic 3-peak shape of the L_3 XMCD of magnetite. Furthermore, there appears to be statistically significant variations in the 3 individual components among the four single magnetosomes sampled, suggesting that crystal-to-crystal variations within a single chain of magnetosomes could be detected with this approach. The crystal-to-crystal variations in the XMCD spectral shape are most likely due to nonstoichiometric occupancies in the three Fe sites — d^6 O_h, d^5 T_d, and d^5 O_h. The non-stoichiometry is due to vacant cation sites in the structure, which arise from either oxidation or conversely, under-oxidation, of Fe (II) to Fe (III), thereby, leading to a charge imbalance (Coker et al., 2007). In the case of oxidation of Fe (II) to Fe (III), a structure having the formula, $(Fe^{3+})[Fe^{2+}{}_{1-3\delta}Fe^{3+}{}_{1+2\delta}\Delta_\delta]O_4^{2-} = Fe_{3-\delta}O_4$ would result, in which the parentheses and square brackets indicate tetrahedral and octahedral sites, respectively, and δ represents the deviation from stoichiometry due to cation vacancies (Pearce et al., 2006). Since the magnetosome crystals were studied in intact bacterial cells, it is of interest to speculate how and when the magnetosome(s) could undergo oxidation. Under what conditions might the magnetite in magnetosomes in intact cells be stoichiometric ? Is it possible that the observed non-stoichiometry is an artifact of sample preparation and air exposure? These and other questions will be investigated in future studies.

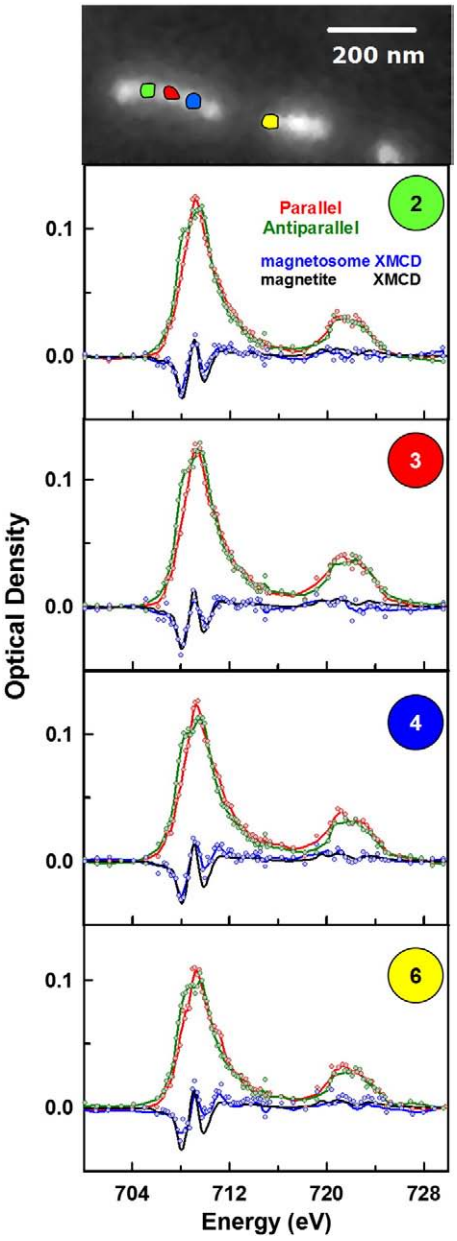

Fig. 5. Spectra of 4 individual magnetosomes in the horizontal chain — at both circular polarizations of light, with the resulting XMCD signal (on the same OD scale) superimposed on a scaled XMCD signal of magnetite (Goering et al., 2007). The image at the top identifies the areas of each of the individual magnetosomes from which these four spectra were obtained.

4. Discussion

This work has presented the first spatially-resolved observation of the magnetism of individual magnetosomes using XMCD signals measured by STXM. Comparison of the XMCD spectra of magnetosome chains to that of abiotic magnetite confirmed the mineral character of MV-1 magnetosomes, showed that the magnetization is essentially saturated, and revealed an off-stoichiometry distribution of oxidation states, which had previously been seen in bulk XMCD measurements of biogenic magnetite. These results demonstrate that STXM has the sensitivity to measure the XMCD signal of single magnetosomes. Most previous bulk studies of XMCD of magnetosomes have been carried out with total electron yield detection, which is highly surface sensitive, raising questions of possible modifications from sample oxidation. The transmission signal recorded by STXM fully samples all of the magnetosome and thus is less sensitive to such effects. At present the quality of the STXM-XMCD data is limited more by systematic than random errors. It will be greatly improved when the measurements are made by alternating between right and left circular polarization at each photon energy (i.e. a time delay of minutes between images recorded at the opposite polarizations, as opposed to the multiple hour delay, which was the case for this study).

These results show that the STXM-XMCD technique is a sensitive tool that can determine the direction of magnetic moments at the nanoscale. With further improvements it should be possible to perform quantitative vector mapping of magnetic moments in individual magnetosomes. Applying that capability to studies of immature magnetotactic cells containing under-developed magnetite crystals, to strains with induced doping of magnetosomes (Staniland et al., 2008; Keim et al., 2009; Kundu et al., 2009), and to different MTB species, will help better understand biomineralization by magnetotactic bacteria. The technique could also be applied to abiotic or other biological nanomagnetic systems.

Acknowledgements

This work was supported by NSERC (Canada) (Hitchcock) and by U.S. National Science Foundation grant EAR-0920718 (Bazylinski). We

thank Dr. Eberhard Goering for supplying the Fe $L_{2,3}$ spectra of magnetite and Gerrit van der Laan for a helpful critical reading of a draft. Olav Hellwig and Eric Fullerton (Hitachi Global Storage Technologies) and Jeff Kortright (Lawrence Berkeley National Lab) provided synthetic out-of-plane magnetized (Pt-Co) multilayer and FeGd samples which were very useful in developing the STXM-XMCD methodology. The Canadian Light Source is supported by the Canada Foundation for Innovation (CFI), NSERC, Canadian Institutes of Health Research (CIHR), National Research Council (NRC) and the University of Saskatchewan.

References

Ade, H., Hitchcock, A.P., 2008. NEXAFS microscopy and resonant scattering: composition and orientation probed in real and reciprocal space. Polymer 49, 643–675.

Albrecht, M., Janke, V., Sievers, S., Siegner, U., Schüler, D., Heyen, U., 2005. Scanning force microscopy study of biogenic nanoparticles for medical applications. J. Magn. Magn. Mater. 290–291, 269–271.

Arato, B., Szanyi, Z., Flies, C., Schüler, D., Frankel, R.B., Buseck, P.R., Pósfai, M., 2005. Crystal size and shape distributions of magnetite from uncultured, magnetotactic, bacteria, and magnetite as a potential biomarker. Am. Mineral. 90, 1233–1241.

Arenholz, E., van der Laan, G., Chopdekar, R.V., Suzuki, Y., 2006. Anisotropic X-ray magnetic linear dichroism at the Fe $L_{2,3}$ edges in Fe_3O_4. Phys. Rev. B 74 094407-(1-7).

Balkwill, D.L., Maratea, D., Blakemore, R.P., 1980. Ultrastructure of a magnetotactic spirillum. J. Bacteriol. 141, 1399–1408.

Bazylinski, D.A., 1996. Controlled biomineralization of magnetic minerals by magnetotactic bacteria. Chem. Geol. 132, 191–198.

Bazylinski, D.A., Frankel, R.B., 2003. Biologically controlled mineralization in prokaryotes. In: Dove, P.M., De Yoreo, J.J., Weiner, S. (Eds.), Biomineralization. Reviews in Mineralogy, vol. 54. Mineralogical Society of America, Washington, D.C., pp. 95–114.

Bazylinski, D.A., Frankel, R.B., 2004. Magnetosome formation in prokaryotes, Nature Rev. Microbiol. 2, 217–230.

Bazylinski, D.A., Dean, A.J., Williams, T.J., Long, L.K., Middleton, S.L., Dubbels, B.L., 2004. Chemolithoautotrophy in the marine, magnetotactic bacterial strains MV-1 and MV-2. Arch. Microbiol. 182, 373–387.

Blakemore, R.P., 1975. Magnetotactic bacteria. Science 190, 377–379.

Blakemore, R.P., 1982. Magnetotactic bacteria. Annu. Rev. Microbiol. 36, 217–238.

Blakemore, R.P., Short, K.A., Bazylinski, D.A., Rosenblatt, C., Frankel, R.B., 1985. Microaerobic conditions are required for magnetite synthesis within *Aquaspirillum magnetotacticum*. Geomicrobiol. J. 4, 53–71.

Brice-Profeta, S., Arrio, M.-A., Tronc, E., Letard, I., Cartier dit Moulin, C., Sainctavit, P., 2005. XMCD investigation of spin disorder in γ-Fe_2O_3 nanoparticles at the Fe $L_{2,3}$ edges. Phys. Scr. T115, 626–628.

Butler, R.F., Banerjee, S.K., 1975. Theoretical single-domain size range in magnetite and titanomagnetite. J. Geophys. Res. 80, 4049–4058.

Carvallo, C., Sainctavit, P., Arrio, M.-A., Menguy, N., Wang, Y., Ona-Nguema, G., Brice-Profeta, S., 2008. Biogenic vs. abiogenic magnetite nanoparticles: a XMCD study. Am. Mineral. 93, 880–885.

Chang, S.-B.R., Stolz, J.F., Kirschvink, J.L., Awaramik, S.M., 1989. Biogenic magnetite in stromatolites. II. Occurrence in ancient sedimentary environments. Precambrian Res. 43, 305–315.

Chen, J., Huang, D.J., Tanaka, A., Chang, C.F., Chung, S.C., Wu, W.B., Chen, C.T., 2004. Magnetic circular dichroism in Fe 2*p* resonant photoemission of magnetite. Phys. Rev. B 69 085107/1-8.

Coker, V.S., Pearce, C.I., Lang, C., van der Laan, G., Pattrick, R.A.D., Telling, N.D., Schüler, D., Arenholz, E., Lloyd, J., 2007. Cation site occupancy of biogenic magnetite compared to polygenic ferrite spinels determined by X-ray magnetic circular dichroism. Eur. J. Mineral. 19, 707–716.

Coker, V.S., Telling, N.D., van der Laan, G., Pattrick, R.A.D., Pearce, C.I., Arenholz, E., Tuna, F., Winpenny, R., Lloyd, J.R., 2009. Harnessing the extracellular bacterial production of nanoscale cobalt ferrite with exploitable magnetic properties. ACS Nano 3, 1922–1928.

de Castro, A.R.B., Fonseca, P.T., Pacheco, J.G., da Silva, J.C.V., da Silva, E.G.L., Santana, M.H.A., 2001. L-edge inner shell spectroscopy of nanostructured Fe_3O_4. J. Magn. Magn. Mater. 233, 69–73.

Dean, A.J., Bazylinski, D.A., 1999. Genome analysis of several magnetotactic bacterial strains using pulsed-field gel electrophoresis. Curr. Microbiol. 39, 219–225.

Devouard, B., Posfai, M., Hua, X., Bazylinski, D.A., Frankel, R.B., Buseck, P.R., 1998. Magnetite from magnetotactic bacteria size distributions and twinning. Am. Mineral. 83, 1387–1399.

Dubbels, B.L., Dispirito, A.A., Morton, J.D., Semrau, J.D., Neto, J.N.E., Bazylinski, D.A., 2004. Evidence for a copper-dependent iron transport system in the marine, magnetotactic bacterium strain MV-1. Microbiology 150, 2931–2945.

Dunin-Borkowski, R.E., McCartney, M.R., Frankel, R.B., Bazylinski, D.A., Pósfai, M., Buseck, P.R., 1998. Magnetic microstructure of magnetotactic bacteria by electron holography. Science 282, 1868–1870.

Dunlop, D.J., 1973. Superparamagnetic and single-domain threshold sizes in magnetite. J. Geophys. Res. Solid Earth 78, 1780–1793.

Egli, R., 2004. Characterization of individual rock magnetic components by analysis of remanance curves, 1. Unmixing natural sediments. Stud. Geophys. Geod. 48, 391–446.

Frankel, R.B., Blakemore, R.P., 1980. Navigational compass in magnetic bacteria. J. Magn. Magn. Mater. 15–18, 1562–1564.

Frankel, R.B., Blakemore, R.P., Wolfe, R.S., 1979. Magnetite in freshwater magnetic bacteria. Science 203, 1355–1357.

Goering, E., Gold, S., Lafkioti, M., Schütz, G., 2006. Vanishing Fe 3d orbital moments in single-crystalline magnetite. Europhys. Lett. 73, 97–103.

Goering, E.J., Lafkioti, M., Gold, S., Scheutz, G., 2007. Absorption spectroscopy and XMCD at the Verwey transition of Fe_3O_4. J. Magn. Magn. Mater. 310, e249–e251.

Heywood, B.R., Bazylinski, D.A., Garratt-Reed, A.J., Mann, S., Frankel, R.B., 1991. Controlled biosynthesis of greigite (Fe_3S_4) in magnetotactic bacteria. Naturwissenschaften 77, 536–538.

Hitchcock, A.P., Morin, C., Zhang, X., Araki, T., Dynes, J.J., Stover, H., Brash, J.L., Lawrence, J.R., Leppard, G.G., 2005. Soft X-ray spectromicroscopy of biological and synthetic polymer systems. J. Electron Spectrosc. 144–147, 259–269.

Howells, M., Jacobsen, C., Warwick, T., 2007. Principles and applications of zone plate X-ray microscopes. In: Hawkes, P.W., Spence, J.C.H. (Eds.), Science of Microscopy. Springer, NY.

Huang, D.J., Chang, C.F., Jeng, H.-T., Guo, G.Y., Lin, H.-J., Wu, W.B., Ku, H.C., Fujimori, A., Takahashi, Y., Chen, C.T., 2004. Spin and orbital magnetic moments of Fe_3O_4. Phys. Rev. Lett. 93 077204/1-4.

Jacobsen, C., Wirick, S., Flynn, G., Zimba, C., 2000. Soft X-ray microscopy from image sequences with sub-100 nm spatial resolution. J. Microsc. 197, 173–184.

Johansson, G.A., Tyliszczak, T., Mitchell, G.E., Keefe, M., Hitchcock, A.P., 2007. Three dimensional chemical mapping by scanning transmission X-ray spectromicroscopy. J. Synchrotron Radiat. 14, 395–402.

Kaznatcheev, K.V., Karunakaran, C., Lanke, U.D., Urquhart, S.G., Obst, M., Hitchcock, A.P., 2007. Soft X-ray spectromicroscopy beamline at the CLS commissioning results. Nucl. Instrum. Methods A 582, 96–99.

Keim, C.N., Lins, U., Farina, M., 2009. Manganese in biogenic magnetite crystals from magnetotactic bacteria. FEMS Microbial. Lett. 292, 250–253.

Kilcoyne, A.L.D., Tylisczak, T., Steele, W.F., Fakra, S., Hitchcock, P., Franck, K., Anderson, E., Harteneck, B., Rightor, E.G., Mitchell, G.E., Hitchcock, A.P., Yang, L., Warwick, T., Ade, H., 2003. Interferometrically controlled scanning transmission microscopes at the advanced light source. J. Synchrotron Radiat. 10, 125–136.

Kim, B.Y., Kodama, K.P., Moeller, R.E., 2005. Bacterial magnetite produced in water column dominates lake sediment mineral magnetism: Lake Ely, USA. Geophys. J. Int. 163, 26–37.

Kirschvink, J.L., Lowenstam, H.A., 1979. Mineralization and magnetization of chiton teeth: paleomagnetic, sedimentologic, and biologic implications of organic magnetite. Earth Planet. Sci. Lett. 44, 193–204.

Komeili, A., Vali, H., Beveridge, T.J., Newman, D.K., 2004. Magnetosome vesicles are present before magnetite formation, and MamA is required for their activation. Proc. Natl. Acad. Sci. U.S.A. 101, 3839–3844.

Komeili, A., Li, Z., Newman, D.K., Jensen, G.J., 2006. Magnetosomes are cell membrane invaginations organized by the actin-like protein MamK. Science 311, 242–245.

Kuiper, P., Searle, B.G., Duda, L.-C., Wolf, R.M., van der Zaag, P.J., 1997. Fe $L_{2,3}$ linear and circular magnetic dichroism of Fe_3O_4. J. Electron Spectrosc. 86, 107–113.

Kundu, S., Kale, A.A., Banpurkar, A.G., Kulkarni, G.R., Ogale, S.B., 2009. On the change in bacterial size and magnetosome features for *Magnetospirillum magnetotacticum* (MS-1) under high concentrations of zinc and nickel. Biomaterials 30, 4211–4218.

Lee, Y., Lee, J., Bae, C.J., Park, J.-G., Noh, H.-J., Park, J.-H., Hyeon, T., 2005. Large-scale synthesis of uniform and crystalline magnetite nanoparticles using reverse micelles as nanoreactors under reflux conditions. Adv. Funct. Mater. 15, 503–509.

Letard, I., Sainctavit, P., Menguy, N., Valet, J.-P., Isambert, A., Dekkers, M., Gloter, A., 2005. Mineralogy of greigite Fe_3S_4. Phys. Scr. T115, 489–491.

Lins, U., McCartney, M.R., Farina, M., Buseck, P.R., Frankel, R.B., 2005. Crystal habits and magnetic microstructures of magnetosomes in coccoid magnetotactic bacteria. Appl. Environ. Microbiol. 71, 4902–4905.

Martel, S., Mohammadi, M., Felfoul, O., Lu, Z., Pouponneau, P., 2009. Flagellated magnetotactic bacteria as controlled MRI-trackable propulsion and steering systems for medical nanorobots operating in the human microvasculature. Int. J. Robot. Res. 28, 571–582.

McCartney, M.R., Lins, U., Farina, M., Buseck, P.R., Frankel, R.B., 2001. Magnetic microstructure of bacterial magnetite by electron holography. Eur. J. Mineral. 13, 685–689.

Morrall, P., Schedin, F., Case, G.S., Thomas, M.F., Dudzik, E., van der Laan, G., Thornton, G., 2003. Stoichiometry of $Fe_{3-\delta}O_4(111)$ ultrathin films on Pt(111). Phys. Rev. B 67 214408-1/7.

Moskowitz, B.M., Frankel, R.B., Bazylinski, D.A., 1993. Rock magnetic criteria for the detection of biogenic magnetite. Earth Planet. Sci. Lett. 120, 283–300.

Muxworthy, A.R., Williams, W., 2006. Critical single-domain/multidomain grain sizes in noninteracting and interacting elongated magnetite particles: implications for magnetosomes. J. Geophys. Res. 111, B12S12.

Oldfield, F., 2007. Sources of fine-grained magnetic minerals in sediments: a problem revisited. Holocene 17, 1265–1271.

Pattrick, R.A.D., van der Laan, G., Henderson, C.M.B., Kuiper, P., Dudzik, E., Vaughan, D.J., 2002. Cation site occupancy in spinel ferrites studied by X-ray magnetic circular dichroism developing a method for mineralogists. Eur. J. Mineral. 14, 1095–1102.

Pearce, C.I., Henderson, C.M.B., Pattrick, R.A.D., van der Laan, G., Vaughan, D.J., 2006. Direct determination of cation site occupancies in natural ferrite spinels by $L_{2,3}$ X-ray absorption spectroscopy and X-ray magnetic circular dichroism. Am. Mineral. 91, 880–893.

Petersen, N., von Dobeneck, T., Vali, H., 1986. Fossil bacterial magnetite in deep-sea sediments from the South Atlantic Ocean. Nature 320, 611–615.

Prozorov, T., Mallapragada, S.K., Narasimhan, B., Wang, L., Palo, P., Nilsen-Hamilton, M., Williams, T.J., Bazylinski, D.A., Prozorov, R., Canfield, P.C., 2007. Protein-mediated synthesis of uniform superparamagnetic magnetite nanocrystals. Adv. Funct. Mater. 17, 951–957.

Scheffel, A., Gruska, M., Faivre, D., Linaroudis, A., Plitzko, J.M., Schüler, D., 2006. An acidic protein aligns magnetosomes along a filamentous structure in magnetotactic bacteria. Nature 440, 110–114.

Schüler, D., Baeuerlein, E., 1998. Dynamics of iron uptake and Fe_3O_4 biomineralization during aerobic and microaerobic growth of *Magnetospirillum gryphiswaldense*. J. Bacteriol. 180, 159–162.

Sette, F., Chen, C.T., Ma, Y., Modesti, S., Smith, N.V., 1990. Magnetic circular dichroism studies with soft X-rays. AIP Conf. Proc. 215, 787–795.

Simpson, E.T., Kasama, T., Posfai, M., Buseck, P.R., Harrison, R.J., Dunin-Borkowski, R.E., 2005. Magnetic induction mapping of magnetite chains in magnetotactic bacteria at room temperature and close to the Verwey transition using electron holography. J. Phys. Conf. Ser. 17, 108–121.

Song, H.-P., Li, X.-G., Sun, J.-S., Xu, S.-M., Han, X., 2008. Application of a magnetotactic bacterium, *Stenotrophomonas* sp. to the removal of Au(III) from contaminated wastewater with a magnetic separator. Chemosphere 72, 616–621.

Staniland, S., Ward, B., Harrison, B.A., van der Laan, G., Telling, N., 2007. Rapid magnetosome formation shown by real-time X-ray magnetic circular dichroism. Proc. Natl. Acad. Sci. U.S.A. 104, 19524–19528.

Staniland, S., Williams, W., Telling, N., van der Laan, G., Harrison, A., Ward, B., 2008. Controlled cobalt doping of magnetosomes in vivo. Nat. Nanotechnol. 3, 158–162.

Stöhr, J., 1999. Exploring the microscopic origin of magnetic anisotropies with X-ray magnetic circular dichroism (XMCD) spectroscopy. J. Magn. Magn. Mater. 200, 470–497.

Thomas-Keprta, K.L., Clemett, S.J., Bazylinski, D.A., Kirschvink, J.L., McKay, D.S., Wentworth, S.J., Vali, H., Gibson Jr., E.K., Romanek, C.S., 2002. Magnetofossils from ancient Mars: a robust biosignature in the Martian meteorite ALH84001. Appl. Environ. Microbiol. 68, 3663–3672.

Weiss, B.P., Kim, S.S., Kirschvink, J.L., Kopp, R.E., Sankaran, M., Kobayashi, A., Komeili, A., 2004. Ferromagnetic resonance and low-temperature magnetic tests for biogenic magnetite. Earth Planet. Sci. Lett. 224, 73–89.

Yamasaki, A., Kobori, H., Osawa, H., Nakamura, T., Sugimura, A., 2009. Soft X-ray magnetic circular dichroism study of magnetite nanoparticles. J. Phys. Conf. Ser. 150 042235/1-4.